A METHOD TO USE A CYLINDRICAL LANGMUIR PROBE IN PULSED PLASMA

by

Alex F. Press

APPROVED BY SUPERVISORY COMMITTEE:

_____
Lawrence J. Overzet, Co-Chair

_____
Matthew J. Goeckner, Co-Chair

_____
Roderick A. Heelis

A METHOD TO USE A CYLINDRICAL LANGMUIR PROBE IN PULSED PLASMA

by

ALEX F. PRESS, BS

THESIS

Presented to the Faculty of

The University of Texas at Dallas

in Partial Fulfillment

of the Requirements

for the Degree of

MASTER OF SCIENCE IN

ELECTRICAL ENGINEERING

THE UNIVERSITY OF TEXAS AT DALLAS

August 2017

ACKNOWLEDGMENTS

A METHOD TO USE A CYLINDRICAL LANGMUIR PROBE IN PULSED PLASMA

Alex F. Press, MSEE
The University of Texas at Dallas, 2017

Supervising Professors: Lawrence J. Overzet, Co-Chair
Matthew J. Goeckner, Co-Chair

The use of pulsed plasmas is currently being studied for integrated circuit fabrication as it may reduce defects and allow for processing optimization. It is therefore necessary to study pulsed plasmas, gaining understanding of the time dependence of important plasma parameters. One common method to measure many of these important plasma parameters is with a Langmuir probe. However, the pulsed plasma environment can cause difficulties in resolving correct values of these plasma parameters. This thesis gives a method for using Langmuir probes in pulsed plasma. More specifically, this thesis provides methods to set proper voltage and timing collection parameters needed to produce correct results. Further, this thesis provides an understanding of how a sheath resistance compensated probe must be constructed to accurately measure rapid changes to a plasma.

TABLE OF CONTENTS

LIST OF FIGURES

LIST OF TABLES

CHAPTER 1

WHY PULSED PLASMA

It is estimated that 99% of the visible universe is plasma[1]. Both stars and the solar winds they create are forms of plasma. On earth, numerous plasmas naturally occur, such as the ionosphere, lightning and fire. There are also many plasmas which are used in industrial settings. These include neon signs, fluorescent lamps and arc welders.

Plasmas are also used extensively in integrated circuit (semiconductor) fabrication. Plasma processing was first used in the semiconductor industry in the late '60s as a method to remove photoresist[2]. By the early '70s, N-type metal-oxide-semiconductor (nMOS) logic etch requirements resulted in plasma etch being used in some manufacturing lines[2]. Plasma etching eventually became the major etch process for most integrated circuit manufacturing due to its anisotropic nature.

Plasmas are commonly used in the semiconductor industry to etch rectangular trenches and round vias as they are often the desired etch shapes (Fig. 1.1, a.). Plasma is uniquely suited to etch these shapes due to the naturally occurring plasma "sheath". Sheaths are interfaces between plasma and objects. A major feature of the sheath is an electric field pointing from the plasma into solid surfaces. It forms to balance the flow of negatively and positively charged species from the plasma center. This sheath electric field accelerates positively charged ions from the plasma to the material surface in a direction that is very close to normal. Those bombarding ions therefore generally only hit on the bottom of trenches and vias, and in conjunction with chemical species cause the etch to occur there[3],[4]. Such anisotropic etch, under the correct conditions, forms trenches and vias with straight 90 degree walls.

While ideally, the plasma etch will result in "perfect" trenches and vias, there are a number of ways in which defects can occur. One manner in which defects form is due to the charging of sidewalls and bottoms of trenches. This charging comes from the difference
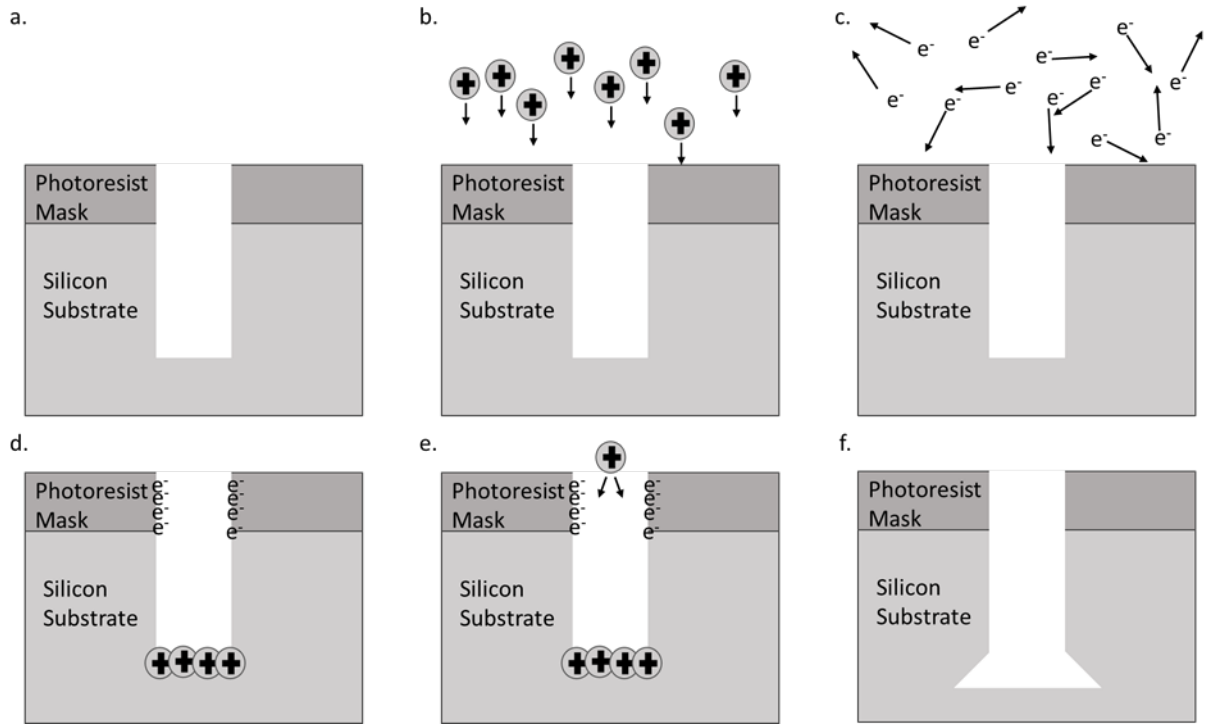
Figure 1.1. (a) Properly formed trench. (b) Trench showing anisotropic ion bombardment. (c) Trench with nearly isotropic electron distribution. (d) Differential trench charging. (e) Ion trajectories with trench charging. (f) Notching due to trench charging.

in angular distributions of bombarding electrons and positive ions (Fig. 1.1, b. and c.). As mentioned, bombarding ions end up with velocities to the surface that are close to normal. The sheath causes the opposite effect on electrons, pushing them back into the plasma bulk. Therefore the electrons that do reach the material, do so with a nearly isotropic distribution. This results in an unbalanced charge being deposited on the trench or via walls and bottom. Most commonly, charging forms as net electrons on the upper walls and net ions at the bottom of the trench (Fig. 1.1, d.). This creates an electric field in the trench which can change the trajectory of the ions and can cause bowing or notching on the sidewalls[5],[6] (Fig. 1.1, e. f.). Furthermore, charge differentials can cause breakdown in thin insulating layers destroying the device[7]. Plasma also creates UV, VUV and x-ray radiation which may

2
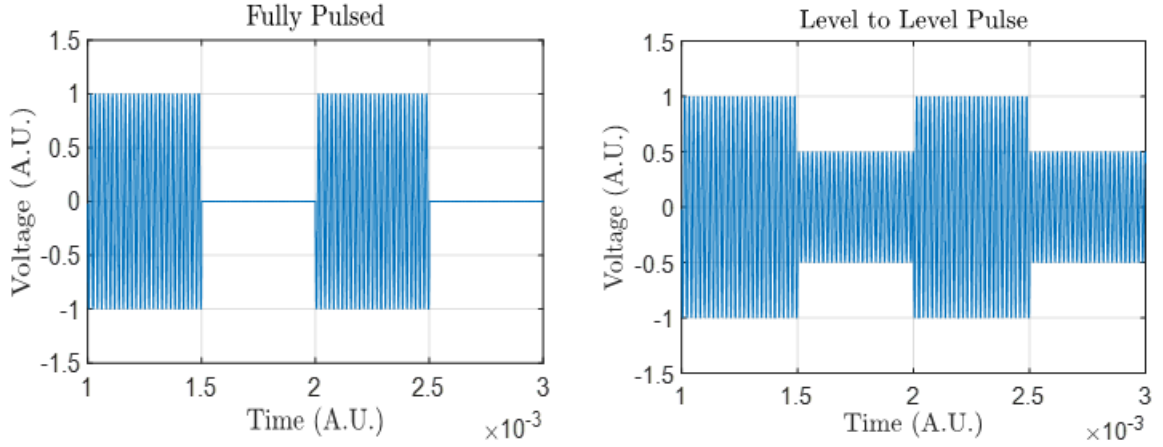
Figure 1.2. (a) Fully pulsed plasma power. (b) Level-to-level pulsed plasma power.

affect trench wall formation[5],[7]. All of these sources must be minimized so as to reduce device damage.

One potential method of reducing plasma-induced damage is to pulse or amplitude-modulate the discharge. This allows for more control than continuous wave (CW) operation because it adds three new ways to tune the processing; (1) the amount by which the power amplitude is modulated, (2) duty cycle and (3) the time scale on which the power amplitude is modulated (pulse frequency). The modulation depth can be set at 0% (CW plasma), 100% (fully pulsed plasma Fig. 1.2 a.) or anywhere in between (level-to-level plasma Fig. 1.2 b.). A level-to-level pulsed plasma is one in which the lower pulse power amplitude is still high enough to maintain the plasma. This mode of pulsing gives two different plasma characteristics but never an off-time. Having this extra control over the plasma gives process engineers more tools to develop processes that produce acceptable results.

Besides adding more control parameters to a process window, pulsing the plasma can help alleviate some defects[8]. During the off-time in a pulsed plasma, the sheath collapses. If given enough time, negative ions and electrons can reach the bottom of trenches and positive ions with broad angular distributions can impact the wall tops helping to neutralize

charging[9]. Finally, during the off-time the plasma is not radiating while reactive radicals and ions can continue to etch and so radiation damage can be reduced[7],[9].

To better understand how these new control parameters affect a process plasma, we separate the effects of amplitude modulation into six major phases as seen in the ion density in Fig. 1.3. For fully pulsed plasma, the first phase is the plasma turn on. This is followed by plasma stabilization and then steady state. These three phases cover the plasma on-time. During the off-time the plasma will start in the initial turn off, followed by a cold, weak residual discharge and finally will be fully dissipated[10]. Both the plasma steady state during the on-time and the fully dissipated state during the off-time are only seen if the on or off periods are long enough. Level-to-level plasma can be broken up into similar time frames referred to as the plasma turn up, high level plasma stabilization, high level plasma steady state, plasma turn down, low level plasma stabilization and the low level plasma steady state.

Although pulsing the plasma can reduce defects, there are some technical issues that must be overcome before it is more widely used in processing. The etch rate often slows during the off-time of the pulse. This can result in longer processing times and lower throughput. The difficulty is further increased because the transition times are characterized by large changes in the plasma conditions and therefore the plasma impedance. Because of this, impedance matching between the power source and the plasma becomes more difficult in pulsed plasmas. To be properly matched, the match network must be able to respond within each pulse.

The purpose of this thesis is to provide background and methodology necessary to accurately measure rapidly changing plasma parameters. In chapter two we review the plasma system and Langmuir probe (LP) diagnostic employed in this study. In chapter three LP theory is presented so as to better understand how plasma parameters are derived from LP measurements. In chapter four the method for using an LP to collect time resolved measure-
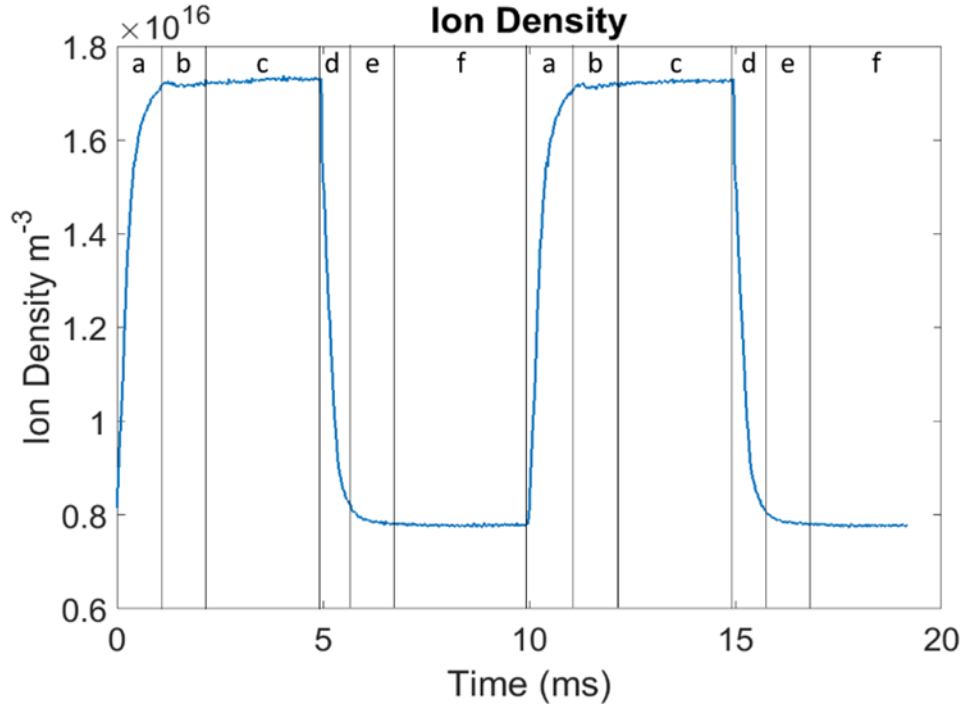
Figure 1.3. Ion density as a function of time in a 100 HZ level-to-level pulsed plasma. (a) Turn up, (b) higher level plasma stabilization, (c) higher level plasma steady state, (d) plasma turn down, (e) lower level plasma stabilization and (f) lower level plasma steady state.

ments in a continuous wave plasma is given. Finally, in chapter five the method for using an LP for time resolved measurements in a pulsed plasma is given.

CHAPTER 2

EXPERIMENTAL SETUP

2.1 Plasma chamber

The plasma reactor used in these studies is the modified gaseous electronics conference chamber (mGEC)[11] shown in Fig. 2.1. The chamber is cylindrical with a 20.1 cm height and 33 cm radius. A capacitively coupled plasma (CCP) source is installed. The powered electrode is at the top and has an 11.4 cm diameter. The bottom electrode is grounded to the chamber walls and has a 15 cm diameter. The electrode gap is adjustable from 1.3 cm to 16.5 cm and was set at 7.6 cm. Gas flows from a perforated 6.4 mm (quarter inch) tube wrapped in a circle immediately above the powered electrode and is pumped out through a port directly below the lower electrode.

Electrically, the plasma system can be modeled as in Fig. 2.2. The circuitry supplying power to the plasma consists of an RF waveform generator (Keysight 33622A), an RF amplifier (ENI A300) and a tunable L-type network. The waveform generator can output a radio frequency (RF) sine wave with frequency up to 120 MHz. In this setup, the RF sine wave was set at 13.56 MHz, a common plasma driving frequency. The sine wave is internally amplitude modulated (AM) using a square wave. The AM square wave was either set at 100 Hz to see all the phases of the pulse or 20 kHz to focus on the transition and stabilization phases. Because an integer number of RF wave periods were equal to the AM wave period, the two signals could be phase locked. Therefore, during the transition periods, the phase of the RF signal could be controlled and was repeatable. The power amplifier has a frequency range from 0.3-35 MHz and max power of 300 watts and is denoted by RF AMP in Fig. 2.2. The L-type matching network allows the circuit load to be impedance matched to the plasma. The matching network consists of two capacitors (C1 and C2) and an inductor (L1). C1 and C2 are variable capacitors and are tuned so that the impedance of the matching network
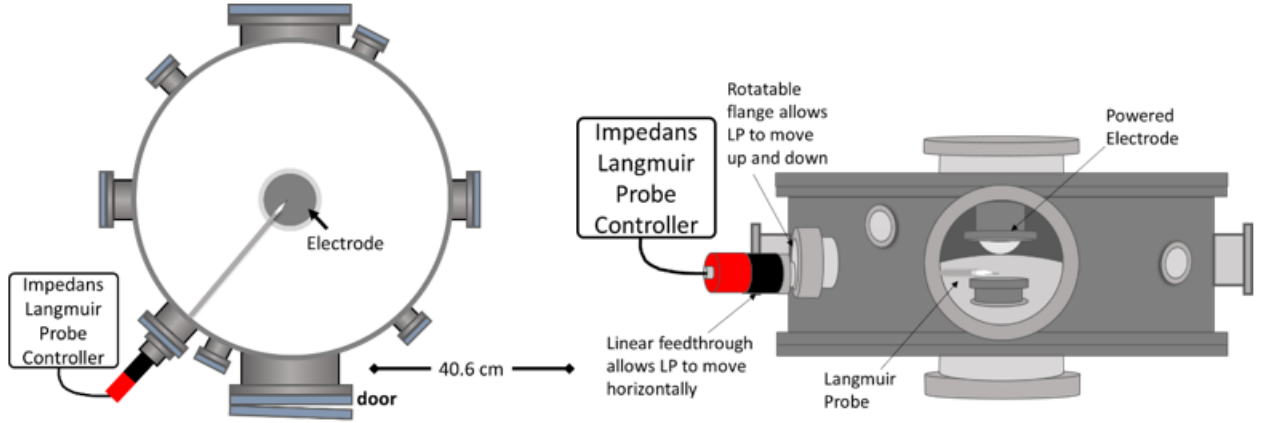
Figure 2.1. Capacitively coupled mGEC with installed Langmuir Probe.
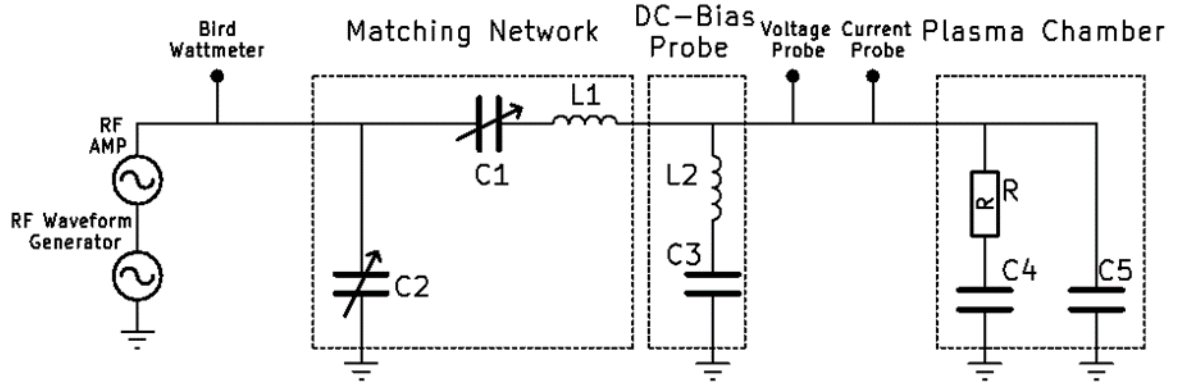
Figure 2.2. Plasma system equivalent circuit.

and power amplifier are close to the impedance of the plasma. This reduces power reflection between the power source and the plasma load. The plasma and chamber can be modeled by R and C4, representing the sheath resistance and capacitance and by C5 representing the stray capacitance between the powered electrode and the grounded chamber.

The power supplied to the plasma is monitored via a number of diagnostics, also shown in Fig. 2.2. A Bird wattmeter measures time-averaged power between the supply and matching network. Between the matching network and plasma chamber there are probes that can be used to temporally resolve the RF supplied current and voltage. These measurements can in

turn be used to calculate both the change in plasma impedance and power delivered during a pulse. These probes are placed as close to the powered electrode as is reasonably possible. This allows the most accurate measurements of the parameters on the electrode. Lastly, a DC bias probe is built into the matching network box and is represented by L2 and C3. L2 has a large inductance that blocks RF power so that the plasma DC bias can be measured as the voltage across C3.

2.2 Diagnostic

The Langmuir Probe is one of the primary tools used in plasma diagnostics. At its most basic, an LP is a conducting wire inserted into a plasma. A voltage relative to the chamber ground is set on the wire using a variable DC source and the resulting current is read out. By sweeping the voltage and measuring the current, a current-voltage (IV) curve is created. The IV curve can then be used to find various plasma parameters such as plasma potential (V_p, the potential in the bulk of the plasma), floating potential (V_f, the voltage at which the net current to an object inserted in the plasma goes to zero), ion saturation current (I_{sat}, current at large negative voltage when few electrons are collected), electron temperature (T_e), electron density (n_e), ion density (n_i) and electron energy probability function.

The LP and software used in these studies was built by Impedans Ltd., and as shown in Fig. 2.3, is made of a ceramic body, DC floating potential pickup, alternating current (AC) ceramic floating potential pickup and tungsten collection tip. The ceramic probe body insulates the probe circuitry from the plasma. The AC ceramic floating potential pickup is coated with metal inside, creating a large capacitive coupling between the plasma sheath and probe tip for RF compensation. The collection tip connects the probe measurement circuit to the plasma. This is the cylindrical collection area for which the current collection theory will be given in the next chapter. For the LP used here, a DC floating potential pickup is
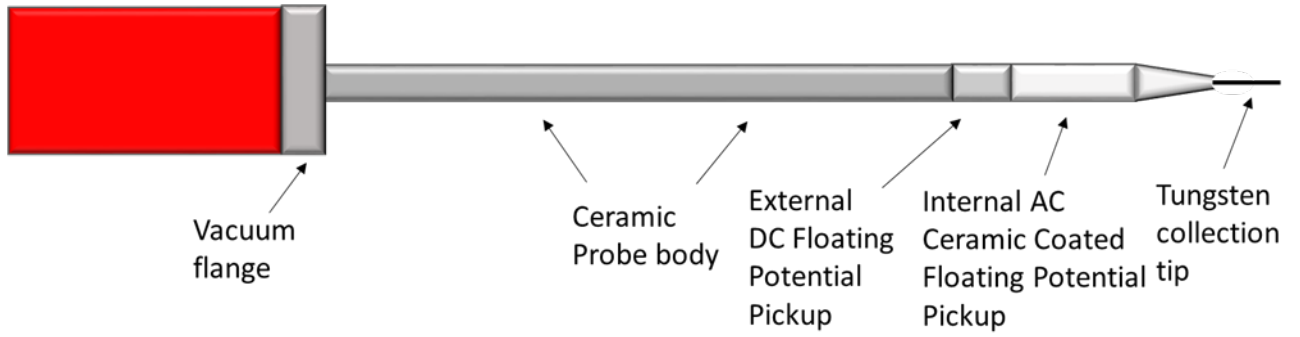
Figure 2.3. Langmuir probe physical description.

used to independently measure the floating potential. This allows the probe to get correct measurements as the plasma sheath resistance changes[12].

As shown in Fig. 2.1, the LP was inserted radially into the chamber. Both the LPs height and radial distance from the center of the electrodes can be adjusted allowing the spatial dependence of plasma parameters to be measured. For these studies, the LP was set at 2.5 cm above the grounded electrode, 5.1 cm below the powered electrode and 1.2 cm from the center radially.

CHAPTER 3

LANGMUIR PROBE THEORY

LP theory bridges the gap between measured IV curves and the fundamental plasma parameters which are being studied in this thesis. Fig. 3.1 gives an example of measured IV curves during four phases of a level-to-level plasma; the turn up phase, the high power steady state phase, the turn down phase and the low power steady state phase. To interpret the measured IV curves like these, thereby properly determining the desired fundamental plasma parameters, it is necessary to understand direct current (DC) probe theory. Three DC theories will be introduced; Orbital Motion Limited[13] (OML), Allen-Boyd-Reynolds[14] (ABR) and Bernstein-Rabinowitz-Laframboise[15],[16] (BRL) theory. The theory used in these studies will then be explained including corrections for ion-neutral collisions in the sheath.

3.1 DC LP theory

To effectively use an LP it is important to understand which theory is most suited for the specific plasma being studied. The theories given above are selected for use based on the plasma charge density, temperature and LP tip size. All three theories assume that ion-neutral collisions are negligible in the sheath but some can be extended to include these types of collisions. Unless stated otherwise, the theories presented here assume a single species, singly ionized, positive plasma. This implies that the current collected by the probe is

$$i(t) = i_{ion}(t) + i_{electron}(t) \tag{3.1}$$

Here i_{ion} is the current due to the ions and $i_{electron}$ is the current due to the electrons. To find some plasma parameters, it is necessary to separate the positive ion current from the negative electron current. This is generally done by finding an expression for the positive ion current and then subtracting it from the total current, resulting in the electron current. This
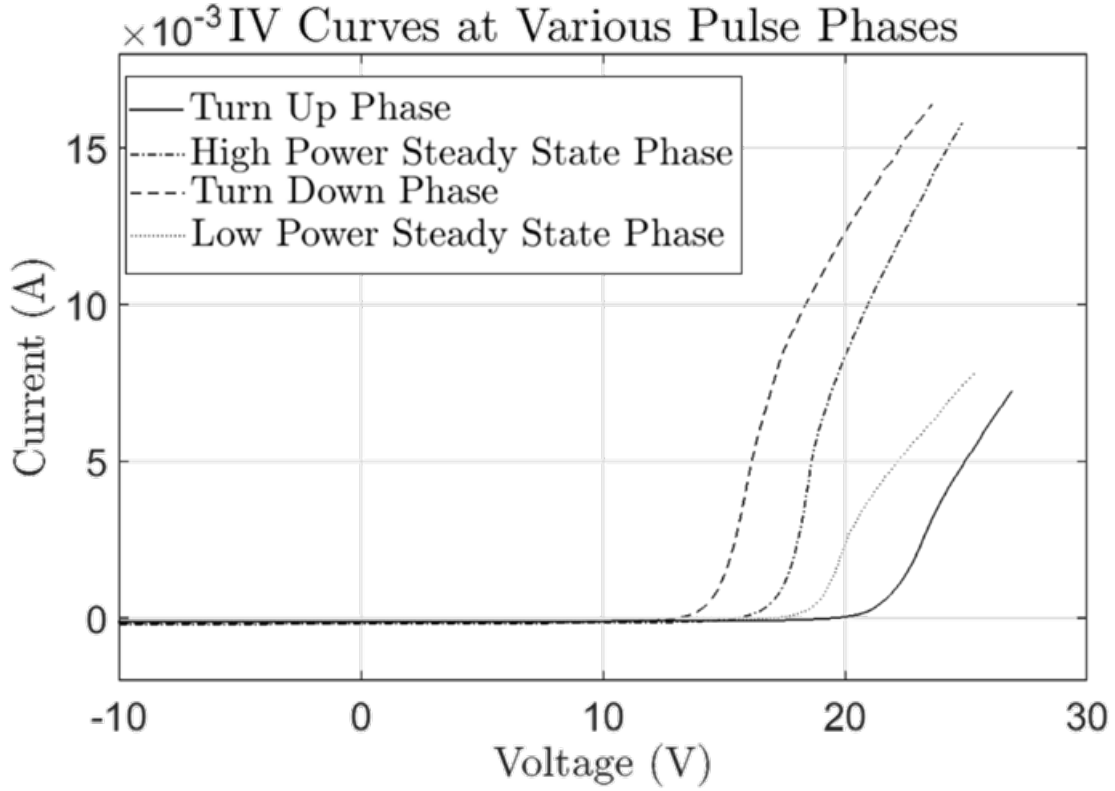
Figure 3.1. IV curves collected at various phases in a 100 Hz pulsed level-to-level Ar plasma.

is in some sense, the motivation of the differences between the various LP theories found in the literature.

Before studying these theories, the concepts of a plasma sheath and V_p must be introduced as they will be used by the theories presented. Because electrons are far less massive, and typically have a higher temperature than ions, they can escape the plasma to a surface much faster than ions. To counter this loss of electrons, and maintain quasineutrality of the plasma, an electric field forms inside the sheath between the plasma and any adjoining surface. This electric field, results in the bulk of the plasma being at a positive electric potential, the plasma potential, relative to adjoining surfaces. Defining the sheath boundary around a plasma is difficult. It is customary to separate the sheath itself into two sections called, the "sheath" and the "presheath". The sheath is characterized by a relatively strong electric field and a substantially lowered density of the repelled charge population. The presheath

has normal densities of both charge populations while still having a weak but non-negligible electric field causing drift in the charge populations.

When the probe is biased more or less negatively relative to the V_p, it will also form an electric field pushing charged particles with the same polarity away, and attract oppositely charged particles. When the probe is biased very negatively relative to V_p ($\geq 30V$), only ions will reach the probe tip. When the probe is biased positively compared to V_p, the tip will collect only electrons. Between those two voltages is a region where both are collected. Furthermore, the ion and electron collection are functions of both the probe voltage and the electron temperature[17].

3.2 Orbital Motion Limited (OML) theory

In the 1920s, H. M. Mott-Smith and Irving Langmuir wrote a series of papers, which were later combined[13], on probe theory that laid out orbital motion limited (OML) theory. This theory uses conservation of the particle's kinetic energy and angular momentum to determine the collected current due to the charge density at the sheath edge and the probe bias. The theory was first developed assuming monoenergetic anisotropic charge carrier distributions, then monoenergetic isotropic charge carrier distributions and finally was extended to Maxwellian charge carrier distributions.

Within this document we will make use of a more recent description of OML theory given by Chen[18]. While this description can be applied to both ion and electron collection, for simplicity, charges are all referred to as ions and the probe bias is either attractive or repulsive. First it is assumed that incoming ions will have an initial velocity v_o, and impact parameter p as shown in Chen[18] Fig. 21 and recreated here in Fig. 3.2. To simplify the mathematics, the probe bias (V_b) is always determined relative to V_p at "infinity" (far from the probe). Further we define R_p as the probe radius and a as the radius of closest approach of an ion with impact parameter p.

Given an ion of mass m and initial velocity of v_o entering the probe sheath, conservation of energy gives

$$\frac{1}{2}mv_o^2 = \frac{1}{2}mv_a^2 + qV_a \equiv -qV_o \tag{3.2}$$

where v_a is the particle velocity at position a, q is the elementary charge, V_a is the potential at point a and V_o as the voltage equivalent of the ion's kinetic energy. Conservation of angular momentum gives

$$pv_o = av_a \tag{3.3}$$

Combining and solving for a in terms of p we get

$$v_a^2 = v_o^2\left(1 + \frac{V_a}{V_o}\right) \tag{3.4}$$

$$a = p\frac{v_o}{v_a} = \frac{p}{\sqrt{1 + \dfrac{V_a}{V_o}}} \tag{3.5}$$

Only those ions for which $a \leq R_p$ will be collected by the probe. The rest will be deflected by the probe and head back into the plasma bulk. For a Maxwellian distribution the random flux is given by

$$\Gamma_r = n_o\sqrt{\frac{k_B T_i}{2\pi m}} \tag{3.6}$$

where n_o is the plasma density in the plasma bulk, k_B is Boltzmann's constant and T_i is the ion temperature. By integrating over all velocities for which $a \leq R_p$, Langmuir and Mott-Smith found the expression for the current to an attractive cylindrical probe

$$i = 2\pi r l \Gamma_r\left(\frac{a}{s}\left[1 - erf\sqrt{\frac{s^2 qV_b}{a^2 - s^2}}\right] + erf\sqrt{\frac{a^2 qV_b}{a^2 - s^2}}\right) \tag{3.7}$$

for $\frac{qV_b}{k_B T_i} < 0$ where s is the sheath width and

$$erfx = \frac{2}{\sqrt{\pi}}\int_x^\infty e^{-y^2}dy \tag{3.8}$$

is the error function. Chen[18] shows that if $s \gg a$ and $T_i \to 0$ this can be reduced to

$$i = 2\pi r l n_o q \frac{\sqrt{2}}{\pi}\sqrt{\frac{qV_b}{m}} \tag{3.9}$$

13
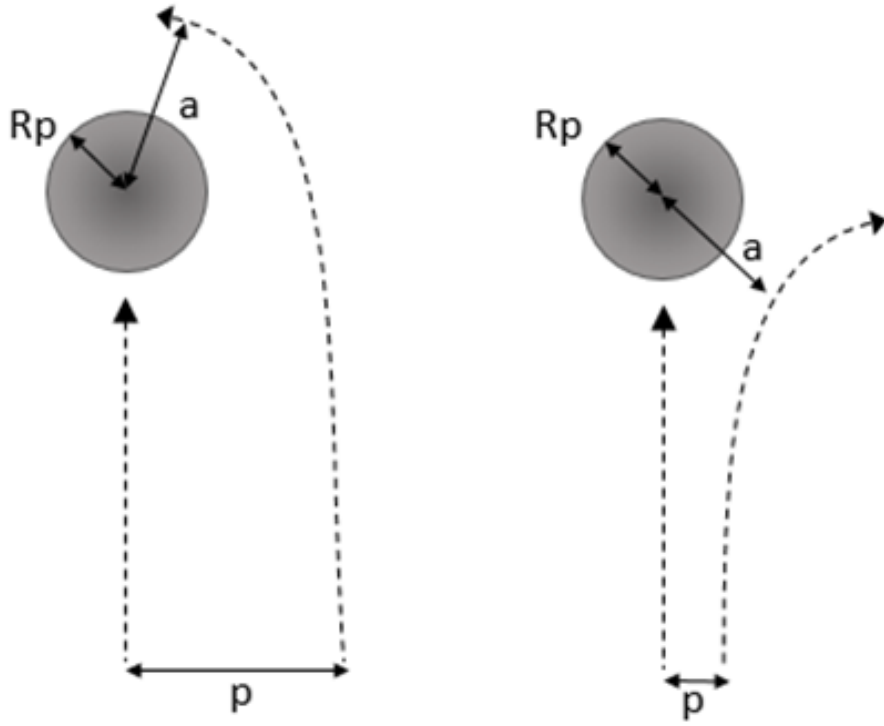
Figure 3.2. Ions approaching an attractive (a) and repulsive (b) probe.

giving the relation

$$i \propto \sqrt{V_b} \qquad (3.10)$$

which is the often quoted form of OML theory.

OML theory usually works for electron collection theory[19]. However, ion collection has been shown to depend on the size of the sheath and therefore the distance of penetration of electric fields into the plasma. The ion current is therefore dependent on T_e and not T_i as shown by Bohm[17]. The assumptions of OML theory make it valid only when the sheath is large compared to the probe radius and the presheath is unimportant[18],[19],[20]. It is generally accepted that this is only a good assumption when the reduced probe radius[21], also called the Debye number[22]

$$\xi_p = \frac{R_p}{\lambda_D} \qquad (3.11)$$

14

is lower than or equal to three[20],[21],[22]. Here R_p is the probe radius and λ_D is the Debye length given by

$$\lambda_D = \sqrt{\frac{\varepsilon_o k_B T_e}{q n_o}} \tag{3.12}$$

where ε_o is the permittivity of free space. For larger Debye numbers, the action of the effects of the sheath must be accounted for in a different way. Therefore other theories have been developed for ion collection.

3.3 Allen-Boyd-Reynolds (ABR) theory

Allen-Boyd-Reynolds (ABR) theory allows for changing sheath width and presheath formation by solving Poisson's equation for all space outside the probe radius. The major assumption of this theory is that the ion temperature (T_i) is equal to zero[18]. Ions therefore only have radial velocity due to the probe bias and there is no orbital motion. The theory was first solved for a spherical probe[14] and then extended for a cylindrical probe[19]. To show the solution for a cylindrical probe we will follow the method shown by Chen[18].

Poisson's equation in cylindrical coordinates gives

$$\frac{1}{r}\frac{\partial V}{\partial r}\left(r\frac{\partial}{\partial r}\right) = \frac{q}{\varepsilon_o}(n_e - n_i) \tag{3.13}$$

To solve Poisson's equation we must develop an understanding of the ion and electron densities. It is assumed that the electron spatial distribution is set by the local potential (V) relative to V_p. By conservation of energy and the assumption of a Maxwellian distribution one finds

$$n_e = n_o e^{\frac{qV}{k_B T_e}} \tag{3.14}$$

To arrive at the ion density it is assumed that the ion flux is conserved. The current flux at any radius is

$$\Gamma(r) = n_i v_i = \frac{\Gamma}{2\pi r} \tag{3.15}$$

15

where Γ is the total ion flux per unit length at the probe surface. By conservation of energy, the ion velocity is given by

$$v_i = \sqrt{\frac{-2qV}{m}} \qquad (3.16)$$

Ion density can then be solved for using

$$n_i = \frac{\Gamma(r)}{v_i} = \frac{\Gamma}{2\pi r}\sqrt{\frac{m}{-2qV}} \qquad (3.17)$$

Plugging these in Poisson's equation we obtain

$$\frac{1}{r}\frac{\partial V}{\partial r}\left(r\frac{\partial}{\partial r}\right) = \frac{q}{\varepsilon_o}\left(\frac{\Gamma}{2\pi r}\sqrt{\frac{m}{-2qV}} - n_o e^{\frac{qV}{k_B T_e}}\right) \qquad (3.18)$$

Rearranging and substituting as shown by Chen[18] we get the ABR equation

$$\frac{\partial}{\partial \xi}\left(\xi\frac{\partial \eta}{\partial \xi}\right) = J\eta^{-\frac{1}{2}} - \xi e^{-\eta} \qquad (3.19)$$

where

$$\xi = \frac{r}{\lambda_D} \qquad (3.20)$$

is the reduced radius,

$$\eta = \frac{-qV_b}{k_B T_e} \qquad (3.21)$$

is the reduced probe voltage and

$$J = \frac{q\Gamma}{2\pi k_B T_e}\sqrt{\frac{m}{2\varepsilon_o n_o}} \qquad (3.22)$$

is the normalized probe current.

The ABR equation can be integrated for a number of J values from $\xi = \infty$ to arbitrarily small values of ξ. Values of η_p can be found from these curves as the point where $\xi = \xi_p$. Now curves can be built for J vs η. At a given probe radius, η is dependent only on parameters we can find from the electron collection region (T_e), well known constants (q, k_B) and the probe bias which is set by the experimenter.

Therefore for a given η the corresponding J is found and since J depends only on known variables, Γ which is the positive current collected at a given probe bias and n_o, the ion density can be found.

While OML theory only produces good results for $\xi_p \leq 3$, ABR theory can give good results for large ξ_p. This is because as probe radius increases compared to the sheath, fewer orbits are possible and the approximation $T_i = 0$ is more accurate.

3.4 Bernstein-Rabinowitz-Laframboise (BRL) theory

To bridge the gap between OML and ABR theory, Bernstein and Rabinowitz[15] (BR) developed a theory that incorporates both orbital motion (non-zero ion temperature) and proper sheath formation for monoenergetic ions[18]. It was then expanded to Maxwellian ion energy distributions by Laframboise[16] (L). Rousseau et al. give the range for which BRL theory is valid as Debye numbers between 5 and 100[20]. Solving Poisson's equation becomes more complex when orbits are introduced, as orbiting ions must be counted twice towards the density distribution at all values of radius grater than its closest approach. This is because any ion not collected will increase the charge density once while headed towards the probe tip and once while headed away[16]. Collected ions are still counted once as they were in ABR theory[18].

Laframboise[16] gives the five equations which are solved to give electric current due to potential bias and charge density. The first is the collisionless steady state Boltzmann equation when there is no gain (ionization) or loss (recombination) of the charged particles given by

$$\frac{df_+}{dt} = \frac{\partial f_+}{\partial \vec{r}} \cdot \vec{v} + \frac{\partial f_+}{\partial \vec{p}} \cdot \vec{F}_+ = 0 \qquad \frac{df_-}{dt} = \frac{\partial f_-}{\partial \vec{r}} \cdot \vec{v} + \frac{\partial f_-}{\partial \vec{p}} \cdot \vec{F}_- = 0 \qquad (3.23)$$

where f_+ is the velocity distribution function of the ions, f_- is the velocity distribution function of the electrons, $\vec{v}$ is the velocity vector, $\vec{p}$ is the momentum vector, $\vec{F}_+$ the Coulombic force on the ions and $\vec{F}_-$ the Coulombic force on the electrons. The second equation is the

force equation with the well-known relationship that the force on a charged particle is equal to its charge times the local electric field given by

$$\vec{F}_+ = -Z_+ q \nabla V \qquad \vec{F}_- = -Z_- q \nabla V \tag{3.24}$$

where Z is the electric charge number of the charged particle. The third is the generalized Poisson's equation given by

$$\nabla^2 V = \frac{-\rho}{\varepsilon_o} \tag{3.25}$$

The fourth is the charge density given by

$$\rho = q(Z_+ N_+ + Z_- N_-) \tag{3.26}$$

The fifth is the number densities given by

$$N_+(\vec{r}) = \int f_+(\vec{r}, \vec{v}) d^3 \vec{v} \qquad N_-(\vec{r}) = \int f_-(\vec{r}, \vec{v}) d^3 \vec{v} \tag{3.27}$$

The solution is found through an iterative procedure. First, a trial function is given for the net charge density (equation 3.24). Second, Poisson's equation (3.23) is then integrated giving the electric potential and its two derivatives. Third, the ion and electron collected currents and the charge density are then calculated. Finally, a numerical method is used to compare and modify the new net charge density with the last. This process is repeated to convergence where the new and old charge densities are equal. Using this method, Laframboise found that V would overshoot and then undershoot the correct solution causing it to diverge. A mixing function found by computational experiment was used to correct for this[16].

To solve the steady state Boltzmann equation, Laframboise used the method employed by Bernstein and Rabinowitz[15]. The difficulty is finding an expression for charge density from a bulk plasma density and distribution function which includes charged particle orbits. As mentioned, charged particles that are not collected by the probe will count twice or not at

18

all for different values of r. A particle which is collected will come from the sheath edge and move with decreasing r until it reaches the probe surface where it is collected. Therefore it will only be counted once in the density calculations. This is what was done in ABR theory. However a charged particle that comes into the probe sheath but then exits without being collected must be accounted for differently. If the radius of closest approach is given by a as it was in the OML theory section, then at all values of r greater than a, the particle must count towards the density once on the way in and once on the way out. The particle will never reach values of r less than a and must not be counted towards the charge density.

To make this possible, the ion velocities are given in terms of the constants of motion; total energy and angular momentum[16]. This negates the need to calculate trajectories of the charged particles when finding an expression for the charge density. Using the symmetry of a cylindrical probe, the probe bias gives a central force field and therefore constants of motion can be found and used in place of the velocity components. The constants of motion used are total energy given by

$$E = ZqV + \frac{m}{2}(v_r^2 + v_t^2) \tag{3.28}$$

where v_r is the radial velocity and v_t is the tangential particle velocity and angular momentum given by

$$J^2 = m^2 r^2 v_t^2 \tag{3.29}$$

Next, the integration from equation 3.27 is changed from velocity space to energy-angular momentum space. In cylindrical coordinates it is given by

$$N(\vec{r}) = \int f(\vec{r}, \vec{v}) dv_r dv_\theta dv_z \tag{3.30}$$

To condense the notation, Laframboise defines the velocity distribution in the z direction as

$$\hat{f}(E, J) = \int_{-\infty}^{\infty} f(E, J, v_z) dv_z \tag{3.31}$$

19

This uses cylindrical symmetry to reduce the density equation from tracking three dimensions to tracking two. To find the charge density in energy-angular momentum space it must be converted from velocity space using

$$N(\vec{r}) = \int_{J^2=0}^{J^2=\infty} \int_{\sqrt{E}=-\infty}^{\sqrt{E}=\infty} \hat{f}(E,J) \frac{\partial(v_r, v_\theta)}{\partial(E,J)} dEdJ \tag{3.32}$$

Evaluating the Jacobian $\left(\frac{\partial(v_r, v_\theta)}{\partial(E,J)}\right)$ allows this to be written as

$$N(\vec{r}) = \frac{2}{m^2 r} \int_{J^2=0}^{J^2=\infty} \int_{E=0}^{E=\infty} \frac{\hat{f}_{v_r<0}(E)K(J^2)}{\sqrt{\frac{2}{m}(E-ZqV) - \frac{j^2}{m^2 r^2}}} \tag{3.33}$$

where K is the number of times a charge should be counted for a given angular momentum. Integrating over J, Laframboise found

$$N(\vec{r}) = \frac{2}{m} \int_{E=0}^{E=\infty} dE \hat{f}_{v_r<0}(E) \sum_n Q_n sin^{-1} \sqrt{\frac{J_n^2}{2mr^2(E-ZqV)}} \tag{3.34}$$

where Q_n, given in Laframboise[16], to shorten notation, is dependent on K and is also three integers set by the values of E and J corresponding to the number of times a particle will be counted.

Laframboise finds for a cylindrical probe the current collected by the probe tip per unit length is then

$$I = \frac{4\pi Zq}{m^2} \int_{E=0}^{E=\infty} \hat{f}(E)J(E)dE \tag{3.35}$$

for a Maxwellian distribution

$$\hat{f}(E) = n_o \frac{m}{2\pi k_B T} e^{\frac{-E}{k_B T}} \tag{3.36}$$

The current collected for a given probe bias can now be related to the bulk plasma density.

3.5 Langmuir probes in radio frequency plasmas

The radio frequency (RF) driven plasma environment is more complex than the DC one. In RF plasmas, the LP tip will pick up both conduction (from ion and electron capture)

and displacement current (from the time varying V_p due to the RF power source). Thus the current to the probe tip must now be written as

$$i(t) = i_{ion}(t) + i_{electron}(t) + C\frac{dV_p}{dt} \tag{3.37}$$

where C is the capacitance between the probe tip and the plasma. The displacement current during an RF cycle can have greater effect on the resulting IV curve than the maximum and minimum of the collected conduction current, giving a distorted IV curve. There is currently no method to effectively remove displacement current effects after data collection. However, proper probe construction can compensate for displacement current. This can be done actively, or passively. For active compensation, the displacement current from the power source is measured, matched and canceled out from the signal[23]. For passive compensation, a large capacitance is placed between the plasma and the probe tip allowing the tip to follow the changes in V_p. A series LC circuit which resonates at the RF frequency is then used to block the RF portion of collected current from the measurement portion of the circuit. This will allow the DC conduction current to pass but block the RF displacement current signal. Therefore only the DC signal is measured and DC theory can be applied to the resulting IV curve. Passive compensation is the more common LP measurement technique and is used in these studies.

A circuit diagram is given for a passive RF compensated probe in Fig. 3.3. A voltage is set by the variable DC supply and the resulting current measured forms an IV curve. C1 is a large capacitor to ground that allows alternating current (AC) signals that make it through the blocking circuitry to be dropped instead of measured. LC is the resonant capacitor-inductor RF choke that blocks the RF induced displacement current. C2 is the capacitance that allows the probe tip to follow the varying RF voltage. The plasma to probe tip interface is the sheath. This can be modeled as a parallel circuit consisting of both a capacitance and resistance. It is modeled by RC1 and RC2 in Fig. 3.3.
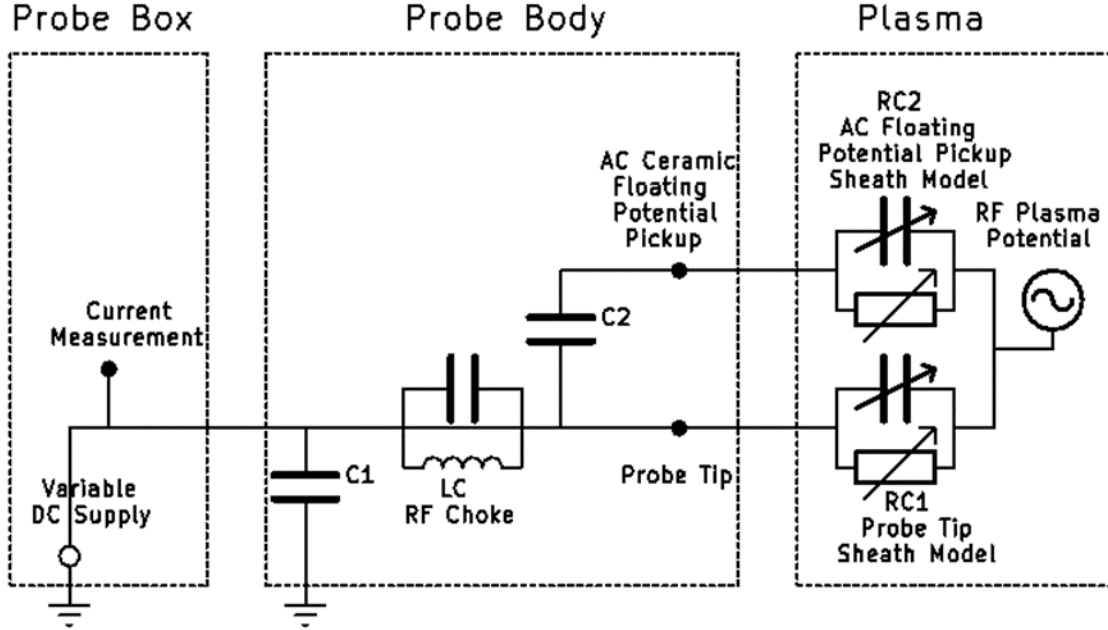
Figure 3.3. Standard RF compensated LP circuit model.

As shown in Fig. 3.4, the probe used in this study has more complex circuitry than the one given in Fig. 3.3. This is because it is designed to block multiple RF frequencies and is compensated for changing sheath resistance. The upper portion of the circuit is modeled shown in Fig. 3.4. This is the standard passively compensated probe circuit but with three RF chokes, blocking three different frequencies. This allows for blocking currents at the power supply frequency as well as at other key frequencies and is modeled by LC1, LC2 and LC3.

The lower portion of the circuit is used to measure the change in V_f, so that sheath resistance can be compensated for in the analysis. C1 is the stray capacitance between the two circuits from the cables connecting the probe body and the probe box as well as the connector on the probe box. The plasma is now also modeled with RC3 which is different from RC2 and RC1 due to different geometries and construction of the electrode pickups.

22
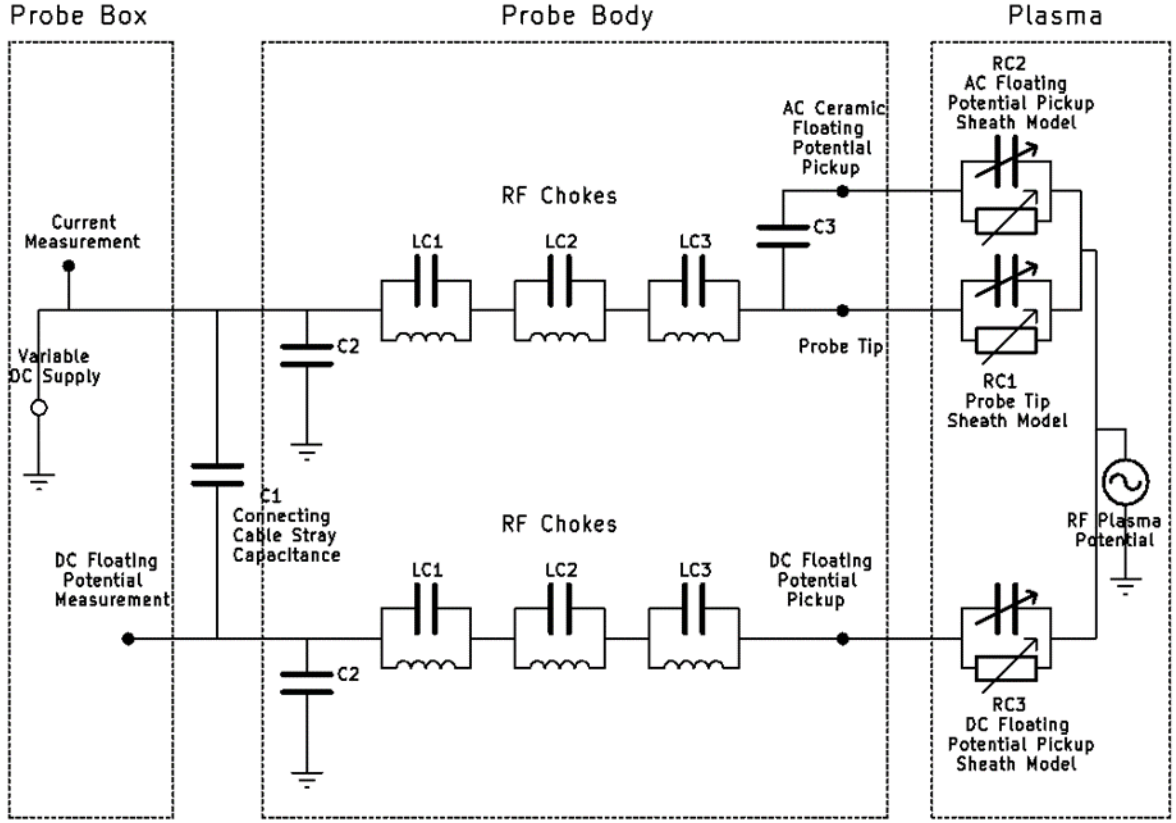
Figure 3.4. RF and varying sheath compensated probe circuit model.

Sheath resistance changes as V_b is swept because, as an LP goes to higher positive bias it pulls in more electrons[12] as shown in Fig. 3.5. Due to current continuity, an equal number of ions must be pulled out of the plasma. To do this, the electric fields in the sheaths around the electrodes must increase in magnitude to cause a higher net ion flux. This perturbation will shift both V_p and V_f to higher values by close to the same amount. Therefore the probe must be compensated to measure this shift. V_f is measured when the probe isn't highly biased and since both V_p and V_f shift by close to the same amount as the probe bias increases, the shift in V_f is measured and the change is subtracted from the applied voltage value. This modified voltage is then used to create the IV curve and therefore give the V_p that would be found in an unperturbed plasma.
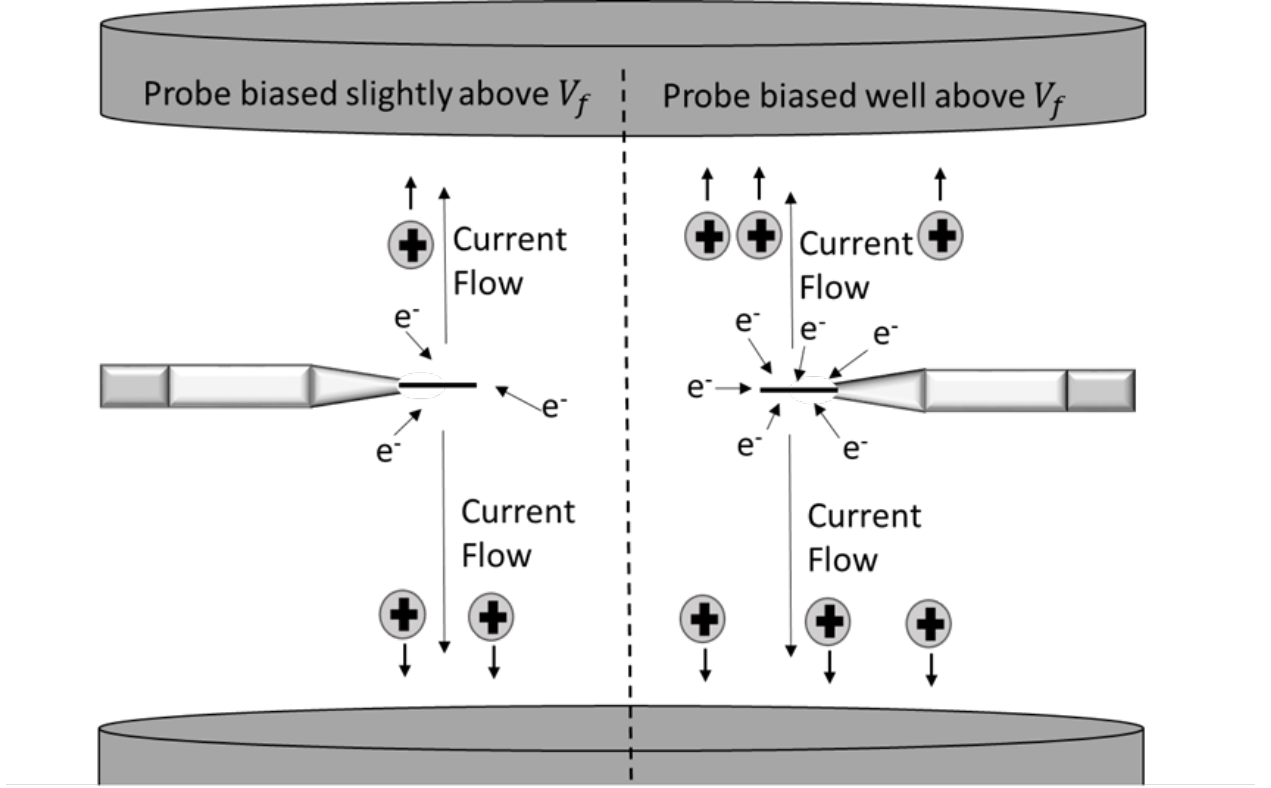
Figure 3.5. Current in a plasma chamber due to a positively biased probe. Left; probe biased slightly above V_f. Right; probe biased well above V_f

3.6 Method used in these studies

Once it is understood how the current is collected, a full IV curve can be studied. As shown in Fig. 3.6 there are three regions of an LP IV curve. The first is the ion saturation region. In this region the probe has been biased negatively with respect to the floating potential. This bias repels virtually all electrons and negative ions and the current collected is due only to positive ion current. The second region is the transition region. As the voltage becomes more positive than the floating voltage, more electrons are collected by the probe. The probe bias is still negative with respect to the plasma potential, and so lower energy electrons are still repelled by the sheath and stay in the bulk. Since the number of electrons captured
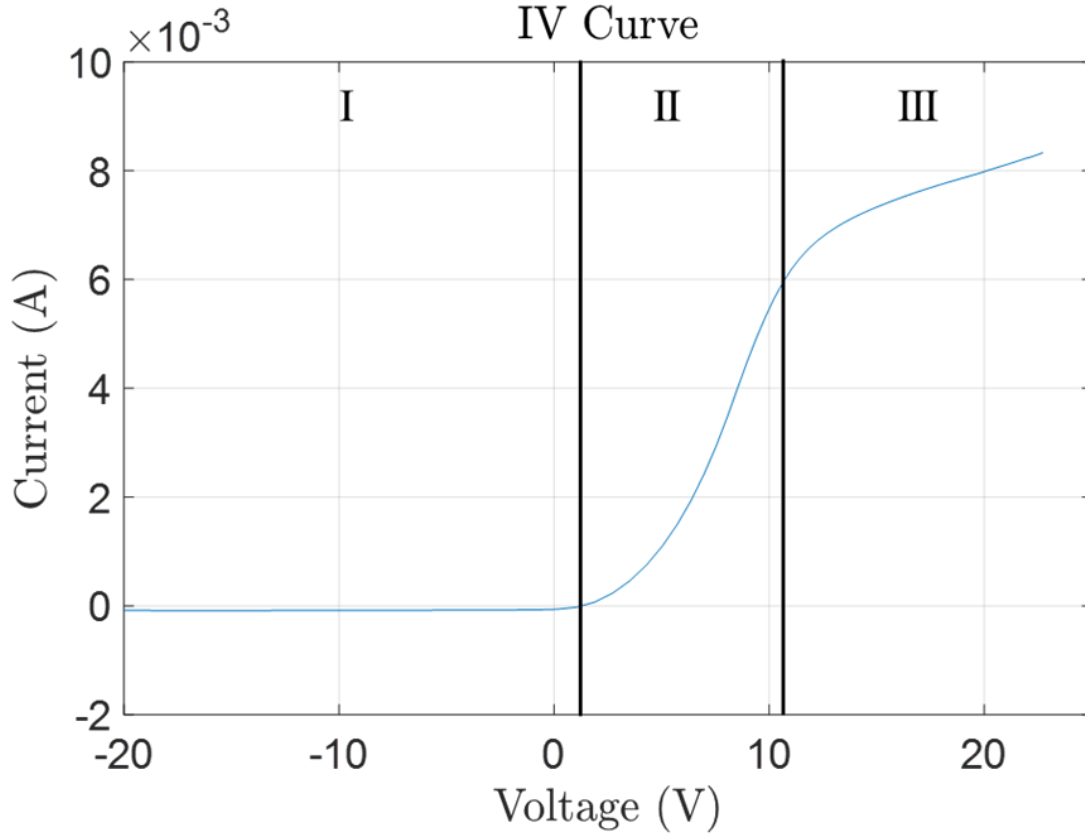
Figure 3.6. IV curve, (I) ion saturation, (II) transition and (III) electron saturation region.

and therefore the current is dependent on the electron energy, the slope of the IV curve in this region can be used to find the electron temperature. The last region is the electron saturation region. Here the probe is biased positively compared to the plasma potential and electrons at any energy are attracted to the probe.

Probe theory can be used to give various plasma parameters. The ones studied here are: plasma potential, floating potential, ion saturation current, electron temperature, electron density, ion density and Debye length.

3.7 Plasma potential

The plasma potential is the point on the curve separating the electron repulsion region and the electron saturation region. This point can be calculated using the intersecting slopes

method[24]. First, the derivative of the IV curve is taken and the voltage and current where the maximum in the derivative occurs is found (V_{max} and $I(V_{max})$). Second, the natural log of ratio of the electron saturation current (I_{esat}) and $I(V_{max})$ is taken. Then the following equation can be used to find V_p

$$V_p = V_{max} + k_B T_e ln\left(\frac{I_{esat}}{I(V_{max})}\right) \tag{3.38}$$

3.8 Floating potential

The floating potential is defined as the point where there is zero net current. This point effectively separates the ion saturation region and the transition region.

3.9 Ion saturation current

The saturation current is the current measured when the probe is biased highly negatively. At this voltage the electron current is negligible and the probe collects only ions.

3.10 Ion and electron current separation

To find the rest of the parameters we must separate the ion current from the electron current in the IV curve. As Chen[18] notes, both ABR and BRL theories can be cumbersome to use. To make them more useful for experiments, parametrized ion current-density relations have been found.

3.11 Collisionless sheath

For collisionless sheaths, BRL theory can be used and the parameterization is given by Narasimhan and Steinbruchel[25]

$$I_{BRL} = \Gamma_o a(\eta)^b \tag{3.39}$$

26
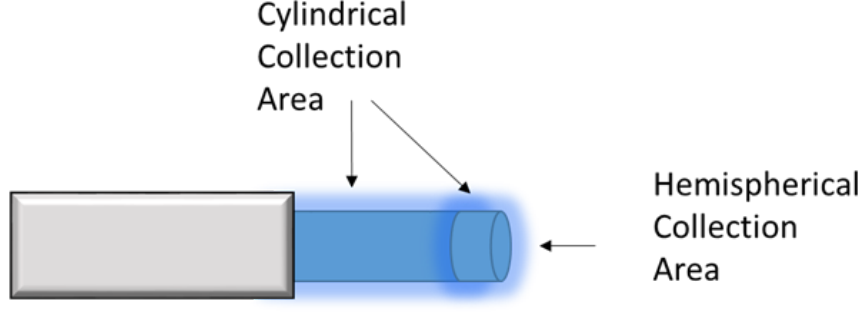
Figure 3.7. Cylindrical and hemispherical probe collection areas

where Γ_o is the ion flux to the edge of the probe sheath. For a cylindrical probe, the current is broken up into cylindrical and hemispherical collection areas as shown in Fig. 3.7. The constants a and b for the cylindrical portion are

$$a = 1.18 - 0.00080\xi_p^{1.35} \tag{3.40}$$

$$b = 0.0684 + (0.722 + 0.928\xi_p)^{-0.729} \tag{3.41}$$

and for the hemispherical "end cap"

$$a = 1.98 + 4.49\xi_p^{-1.31} \tag{3.42}$$

$$b = -2.95 + 3.61\xi_p^{-0.0394} \tag{3.43}$$

The total ion current is then given by

$$I_{BRL} = I_{BRL}(sph) + I_{BRL}(cyl) \tag{3.44}$$

3.12   Collisional sheath

For collisional sheaths the parameterization based on both ABR and BRL theory of Zakrzewski and Kopiczynski[21] is used. The current is given by

$$I = I_{BRL}\gamma_1\gamma_2 \tag{3.45}$$

where γ_1 and γ_2 are collisional terms representing two different physical processes.

γ_1 is a factor representing the increase in ion current due to collisions reducing angular momentum and allowing the charge to flow radially into the attracting probe[21]. γ_1 is given by

$$\gamma_1 = \chi_i\left(\frac{I_{ABR}}{I_{BRL}} - 1\right) \quad \text{for} \quad \chi_i < 1 \tag{3.46}$$

$$\gamma_1 = \frac{I_{ABR}}{I_{BRL}} \quad \text{for} \quad \chi_i > 1 \tag{3.47}$$

where χ_i is the number of ion-neutral collisions in the sheath given by

$$\chi_i = \frac{r_s - r_p}{\lambda_i} \tag{3.48}$$

where λ_i is the mean free path given by

$$\lambda_i = \frac{k_B T_g}{P\sigma_{i-N}} \tag{3.49}$$

where T_g is the neutral temperature, P is the neutral pressure and σ_{i-N} is the ion-neutral cross section. The current relation parameterization I_{ABR} was found by Klagge and Tichy[26] and is given by

$$I_{ABR} = a\left(\frac{\eta}{b}\right)^c \tag{3.50}$$

where a, b and c are given by

$$a = (\xi_p + 0.6)^{0.05} + 0.04 \tag{3.51}$$

$$b = 0.09\left(e^{-\xi_p^{-1}} + 0.08\right) \tag{3.52}$$

$$c = (\xi_p + 3.1)^{-0.6} \tag{3.53}$$

γ_2 is the factor representing a decrease in ion current due to collisions given by

$$\gamma_2 = \frac{3 - 2e^{-\chi_i}}{1 + 2\chi_i} \quad \text{for} \quad \chi_i < 1 \tag{3.54}$$

$$\gamma_2 = \frac{3 - e^{-\chi_i}}{2(1 + 2\chi_i)} \quad \text{for} \quad \chi_i > 1 \tag{3.55}$$

28

In this case elastic scattering of the ions can push them out of the sheath and back into the bulk causing them to not be collected[21].

Once the ion current is found, it can be subtracted from the total current giving the electron current.

$$I_{electron} = I - I_{ion} \tag{3.56}$$

3.13 Electron temperature

From Lieberman[4] we see electron temperature is found using

$$T_e = \frac{V_b}{ln\left(\frac{I_e}{I_{esat}}\right)} \tag{3.57}$$

3.14 Ion density

Ion density can be found as shown by Šícha et al.[27] using

$$n_i = \frac{I_{sat}}{R_p l_p q} \sqrt{\frac{m_i}{2\pi k_B T_e}} \tag{3.58}$$

where l_p is the probe length.

3.15 Electron density

Electron density can be found in the same way as ion density using $I(V_p)$ in place of I_{sat}

$$n_e = \frac{I(V_p)}{R_p l_p q} \sqrt{\frac{m_e}{2\pi k_B T_e}} \tag{3.59}$$

CHAPTER 4

METHOD FOR TIME RESOLVED MEASURMENTS IN CW PLASMA

To find the time dependence of plasma parameters, IV curves must be collected at different times in the pulse cycle. In this chapter the plasma being measured is in CW mode. It is necessary to understand how the system works in CW conditions before moving on to pulsed environments. To illustrate how the system works to collect IV curves at a given time in the pulse cycle, an example is given.

4.1 Timing sweep

A sync signal is generated by a function generator and is sent to the LP box. If the collection cycle is 1 kHz, then so is the sync signal and the period is 1000 μs. The user can then select a start time, an end time and a sampling period over which the current collected is averaged. If the user selects a start time of zero, a sampling period of 10 μs and an end time of 1000 μs there will be current samples taken and averaged from 0-10 μs, 10-20 μs, 20-30 μs... with the last at 990-1000 μs. The result is 100 different current values during a 1 kHz collection cycle.

4.2 Voltage sweep

The user also sets a start, stop and step voltage. If a selection of -20 V, 30 V, 1 V is made then the system will set the probe to -20 V and measure the current for a full cycle, set the probe to -19 V, measure the current for a full cycle and continue until the measurement at 30 V is made. In this way full IV curves are created representing the plasma at various times during the pulse.

To better illustrate how time dependent IV curves are measured, Table 4.1 gives the order in which data is collected. First V_{min} is set on the probe tip. Then the current is collected

Table 4.1. Time resolved IV trace data collection process order and IV curve temporal separation.

	IV curve at T_{start}	IV curve at $T_{start+T_{sample}}$	IV curve at $T_{start+2T_{sample}}$	IV curve at $T_{start+3T_{sample}}$	IV curve at $T_{start+4T_{sample}}$		IV curve at T_{end}
	T_{start}	$T_{start} + T_{sample}$	$T_{start} + 2T_{sample}$	$T_{start} + 3T_{sample}$	$T_{start} + 4T_{sample}$	...	T_{end}
V_{min}	i1	i2	i3	i4	i5	...	in
$V_{min} + V_{step}$	in+1	in+2	in+3	in+4	in+5	...	i2n
$V_{min} + 2V_{step}$	i2n+1	i2n+2	i2n+3	i2n+4	i2n+5	...	i3n
$V_{min} + 3V_{step}$	i3n+1	i3n+2	i3n+3	i3n+4	i3n+5	...	i4n
$V_{min} + 4V_{step}$	i4n+1	i4n+2	i4n+3	i4n+4	i4n+5	...	i5n
$V_{min} + 5V_{step}$	i5n+1	i5n+2	i5n+3	i5n+4	i5n+5	...	i6n
...	...	...	...	...	...	...	i7n
V_{max}	i(m-1)n+1	i(m-1)n+2	i(m-1)n+3	i(m-1)n+4	i(m-1)n+5	i(m-1)n+6	imn

at the start time (i1). After the set time step, in the same pulse, the current is collected again (i2). After another set time step, in the same pulse, the current is collected again (i3). This is continued until the end time is reached and the nth current is collected (in). The voltage is then changed by the set voltage step and the process is repeated collecting currents i(n+1) to i(2n). The voltage is changed again and the process repeats until the currents are collected at V_{max}. The IV curves are then separated by time. Column one forms the IV curve at the start time, column two is the start time plus the set sample time. The pattern is continued until the IV curve at the set end time is found. These IV curves can then be used to find the time dependence of the plasma parameters during the pulse.

4.3 Proper sampling time

Minimizing noise in the plasma parameters calculated from time dependent IV traces, requires picking a sampling period that is an integer multiple of the RF cycle. To illustrate this, if a 0.250 μs sampling period is chosen with a plasma driving frequency of 13.56 MHz (0.0737 μs period) we will have approximately 3.39 RF periods over which each current measurement is integrated. Using this sampling period, noise is seen in the measured plasma parameters. A pattern was detected while inspecting the noise. To better understand the
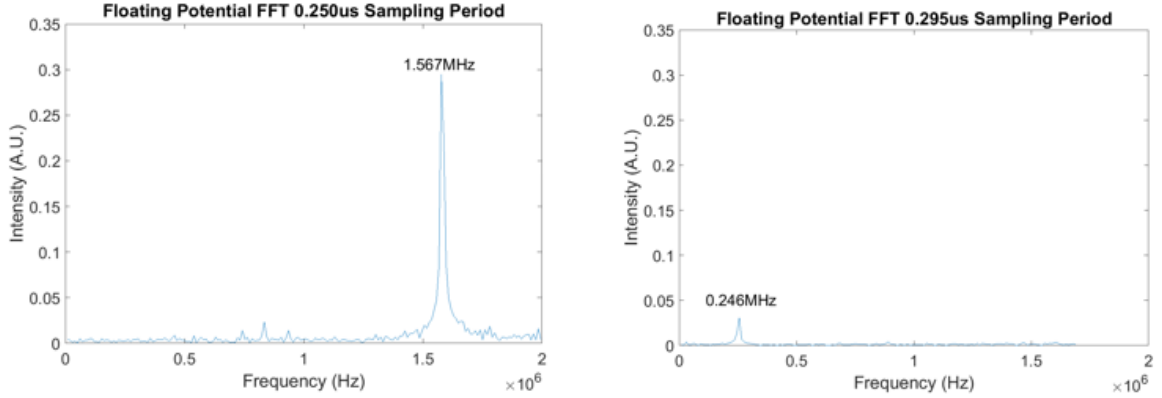
Figure 4.1. Fast Fourier transform (FFT) of the floating potential using sampling periods a. 0.250 μs and b. 0.295 μs with 13.56 MHz RF frequency. Larger peak is associated with larger variation in the IV curves and calculated plasma parameters. As the sampling period gets closer to an integer number of RF periods, it takes longer to repeat and the beat frequency becomes smaller.

nature of this pattern, a Fast Fourier Transform (FFT) was performed on the calculated plasma parameters. Since floating potential is measured simply as the zero crossing on the IV curve, the FFT of the variations in this parameter was found to be the most useful. The results of the FFT demonstrated that there was a beat frequency that was dependent on the sampling period (Fig. 4.1).

It has been found that the magnitude of the beat frequency noise decreased as the sampling period comes closer to an integer number of RF periods, or if longer sampling periods were used. This can be explained by thinking about what integrating over partial RF periods means. During the RF period, the plasma IV curve will vary. Therefore taking a measurement at different times during the period will give different results. If 0.250 μs is selected as the sampling period, with a RF power period of 0.0737 μs (13.56 MHz), then the first measurement will be integrated over the first 3.39 RF cycles. The second sample will be integrated over the last 0.61 RF cycle and the next 2.78 RF cycles (Fig. 4.2 a.). This will give different IV curves and therefore different results between measurements. This causes the noisy results. The reason increasing the sampling period also decreases the noise is as we
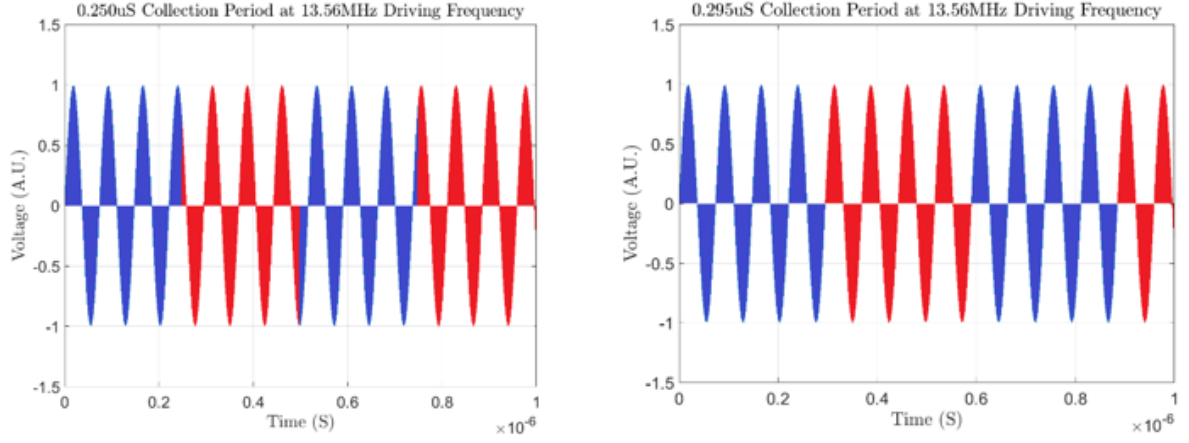
Figure 4.2. First few sampling periods a. 0.250 μs and b. 0.295 μs with 13.56 MHz RF frequency

increase the sampling period, the percentage of partial RF cycles to full RF cycles decreases. The result is the partial RF cycles measured have a smaller effect on the averaged current measurement.

If a sampling period with an integer number of RF cycles is used then this signal can be eliminated. However, this is not fully possible as the period of an RF cycle at 13.56 MHz is $73.746313ns$. We can however choose a sampling period that is close to an integer number of RF cycles (Fig. 4.2 b.). Four RF cycles is very close to 0.295 μs and forty RF cycles is very close to 2.95 μs. Therefore for a fine time step 0.295 μs is used and for longer scans a course time step of 2.95 μs or 29.5 μs is used.

4.4   Proper voltage settings

If the voltage settings, especially the step size and max voltage, are not correct then the calculated plasma potential and electron temperature can also be incorrect. The plasma parameters are not as sensitive to the minimum voltage. If the minimum voltage is set to around -10 or -20 V the ion saturation portion of the curve and the floating voltage are

33

well resolved. The maximum voltage must be set large enough to fully resolve the plasma potential. However if it is too large, two issues can occur. First the LP can drain electrons on the same order as their generation rate, causing large perturbations to the plasma[28]. The LP will then be measuring the disturbed plasma and not the plasma under normal conditions. Secondly as discussed, the way in which the probe compensates for changing sheath resistance can cause the effective voltage step size to be reduced at large positive bias. This will cause the IV curve in this region to have very fine steps on the x axis voltage. Small amounts of naturally occurring noise in the current measurements will then cause the calculated first derivative to vary widely. This in turn causes errors in the measurement of V_p (Fig. 4.3 a.). This second issue is highly dependent on the voltage step size. Picking a larger step size can reduce or eliminate this effect as shown in Fig. 4.3 b. However, as the voltage step size is increased, errors in the measured plasma potential and electron temperature are also induced. Therefore, finding the optimum voltage settings is critical for accurate measurements.

One can determine the best voltage sweep parameters in the following manner. For the first sweep an educated guess is used. The IV curve and its derivative are then inspected. If the derivative has one clear, reasonably narrow and smooth peak without very many data points taken after, then the results are considered acceptable (Fig. 4.3 d.). If the derivative doesn't reach a peak as shown in Fig. 4.3 c., then the maximum voltage is increased. If there are many data points taken after the peak the max voltage is decreased (Fig. 4.3 a. and b.). If the peak looks broad (Fig. 4.3 b.) then the voltage step size is reduced. If the step size is changed, it is often necessary to readjust the maximum voltage.
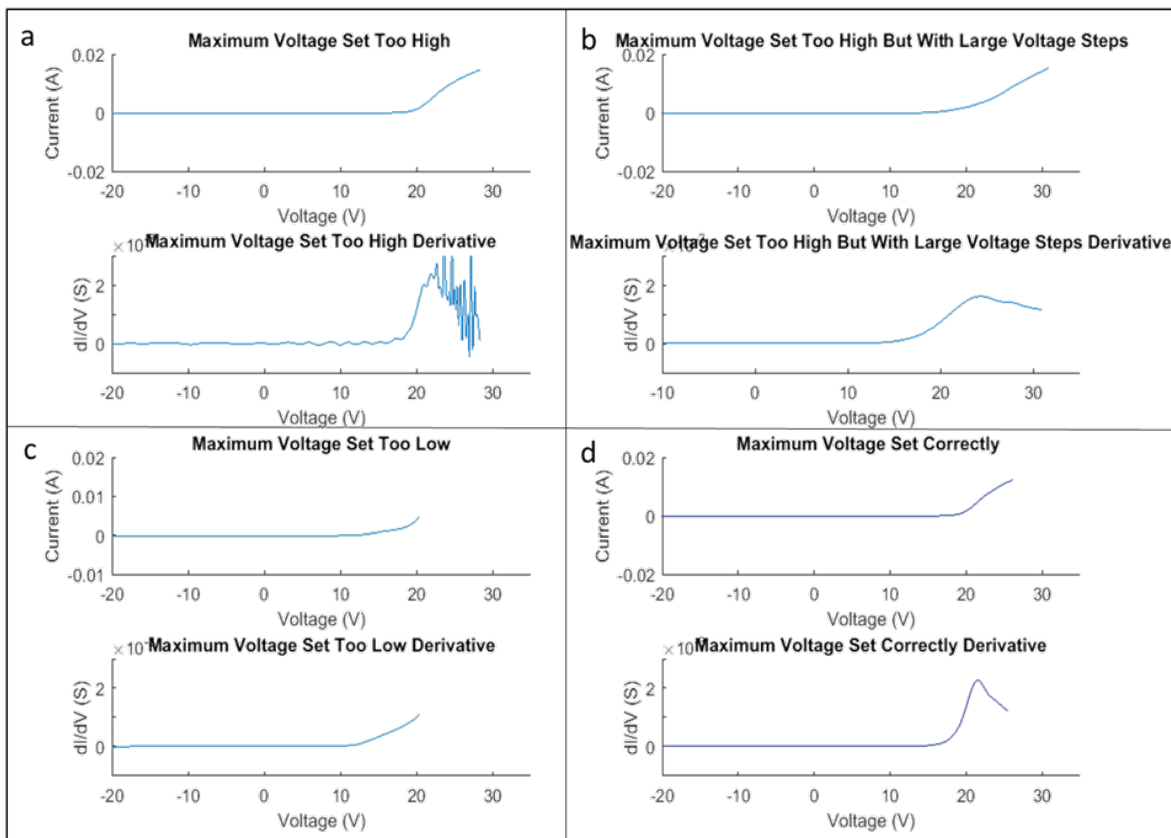
Figure 4.3. IV curves and their derivative with different voltage settings. (a) IV curve with high maximum voltage. (b) IV curve with high maximum voltage and large voltage steps. (c) IV curve with low maximum voltage. (d) IV curve with proper voltage settings.

CHAPTER 5

COLLECTING IV CURVES IN PULSED PLASMAS

Using an LP in pulsed plasmas introduces new difficulties. As seen in Fig. 3.2, at different times in the pulse cycle, the IV curves can be different shapes and sizes. It is then important to subdivide the pulse cycle and set the proper min, max and voltage step for each subdivision. This is done as explained in the previous section, except now each subdivision is looked at separately and optimized. In Fig. 5.1, the measured plasma potential is shown over two pulse cycles. Part a shows the result when the voltages are set using a best guess for the optimal voltage settings. Part b shows the same measurements, but after going through two iterations of improvements, where the voltage settings have been fine tuned for each part of the pulse cycle. This process must be repeated until an optimal result is found.

LPs have been used successfully in pulsed plasma before as seen in Rousseau[29]. However in those studies, the sample period has been large compared to some of the changes in plasma parameters. To better understand these transitions, smaller sampling periods must be used. Minimum possible sampling periods are set by the probe circuitry. As the fundamental drive frequency is blocked, sampling periods must be longer than the RF period. Since the interest of these studies is to measure the change in plasma parameters and to reduce inherent noise, the sampling period was always a minimum of four RF cycles.

In the studies presented here it was found that both V_p and V_f during the turn on or turn up can reach their maximum within 10 μs, and N_e and T_e, can change dramatically in 5 μs. Therefore sampling periods as low as 0.295 μs (four RF periods) give reasonable resolution in the transition regions. However, due to this fast sampling period, and because the LP is compensated for changing sheath resistance, error in the IV curves that may have been averaged out in previous studies or not seen due to different probe construction have been observed.
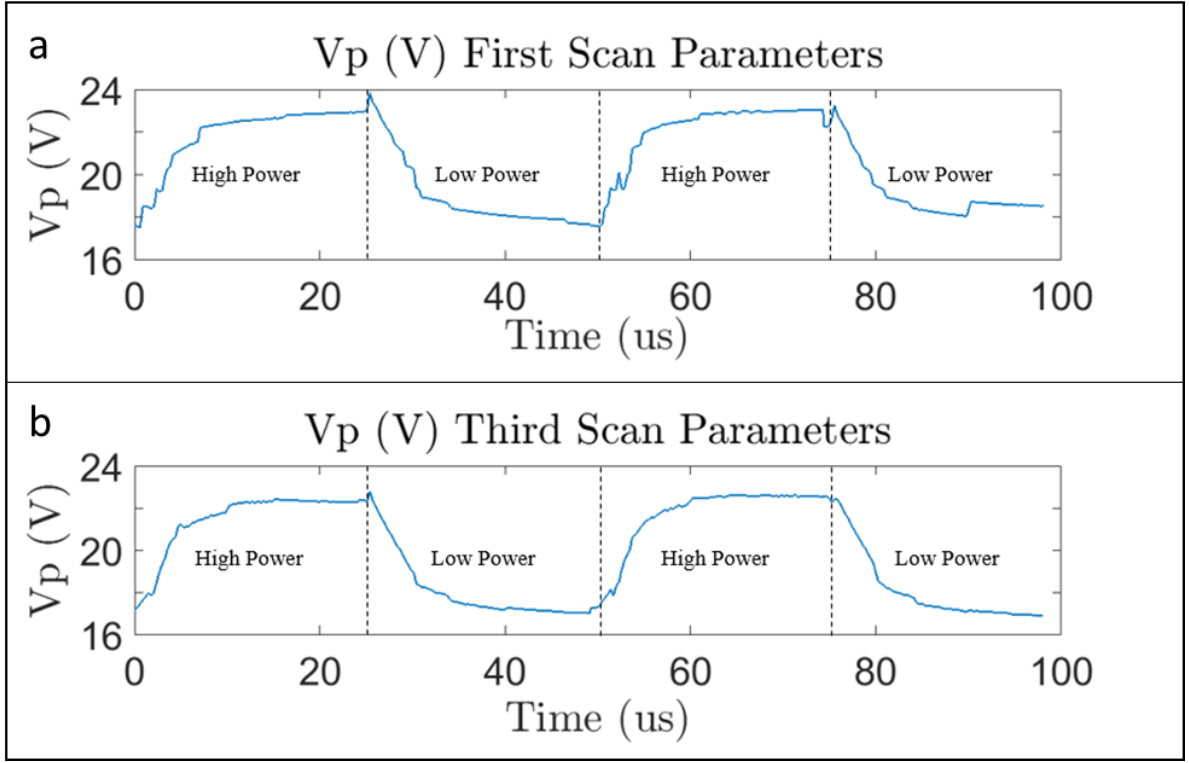
Figure 5.1. (a) Calculated plasma potential without optimized voltage settings. (b) Calculated plasma potential after two cycles of voltage setting optimization.

When measuring pulsed plasma during the transition time, especially the turn on or turn up, the IV curve can be distorted (Fig. 5.2). This distortion is unphysical as there is no explanation for more ion collection or less electron collection at a more positive probe bias. Instead the circuit is picking up displacement current that can swamp the electron and ion currents. As discussed previously, displacement currents caused by changes in the floating and plasma potential can create extra current in the measurement circuit. The displacement currents caused by pulsed plasma transitions are at a frequency lower than the power source RF and consequently are not blocked by the RF chokes. It is not desired to add blocking components at this frequency as they would also block the time dependent features in the IV curve that are being studied.
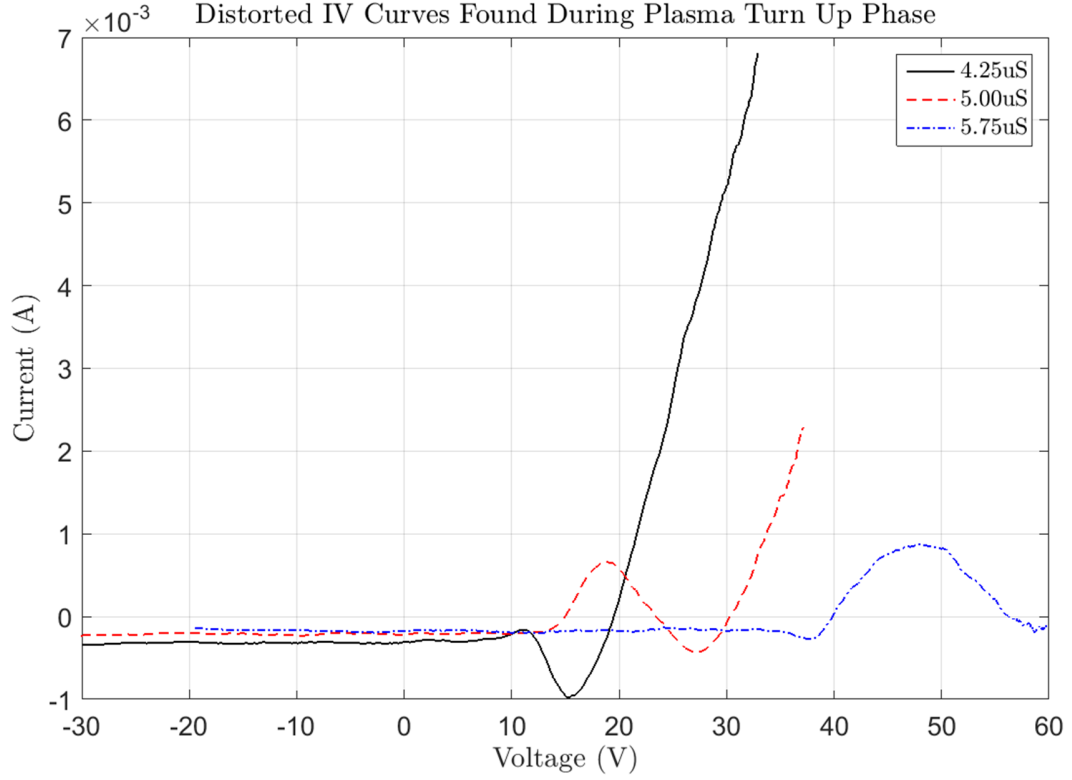
Figure 5.2. Distorted IV curves taken at 4.25, 5.00 and 5.75 μs into the plasma turn up portion of the pulse cycle.

The collected current including this new displacement current can be given by

$$I = I_{ion} - I_{electron} + C\frac{dV_{RF}}{dt} + C1\frac{dV_{pulse}}{dt} \tag{5.1}$$

The last term on the right hand side represents current due to the change in V_f and V_p during the pulse cycle. C1 represents the stray capacitance between the measurement and sheath resistance compensation circuits as shown in Fig. 5.3. As is evident from equation 5.1, this current can be reduced by reducing the capacitance. To do this the LP-plasma circuit is reexamined.

Fig. 5.3 shows the LP circuit model modified to focus on DC collection and the transients introduced by the pulsed plasma rather than the RF displacement current. In the probe body, the model for the LC components are changed to solely inductive components. This is
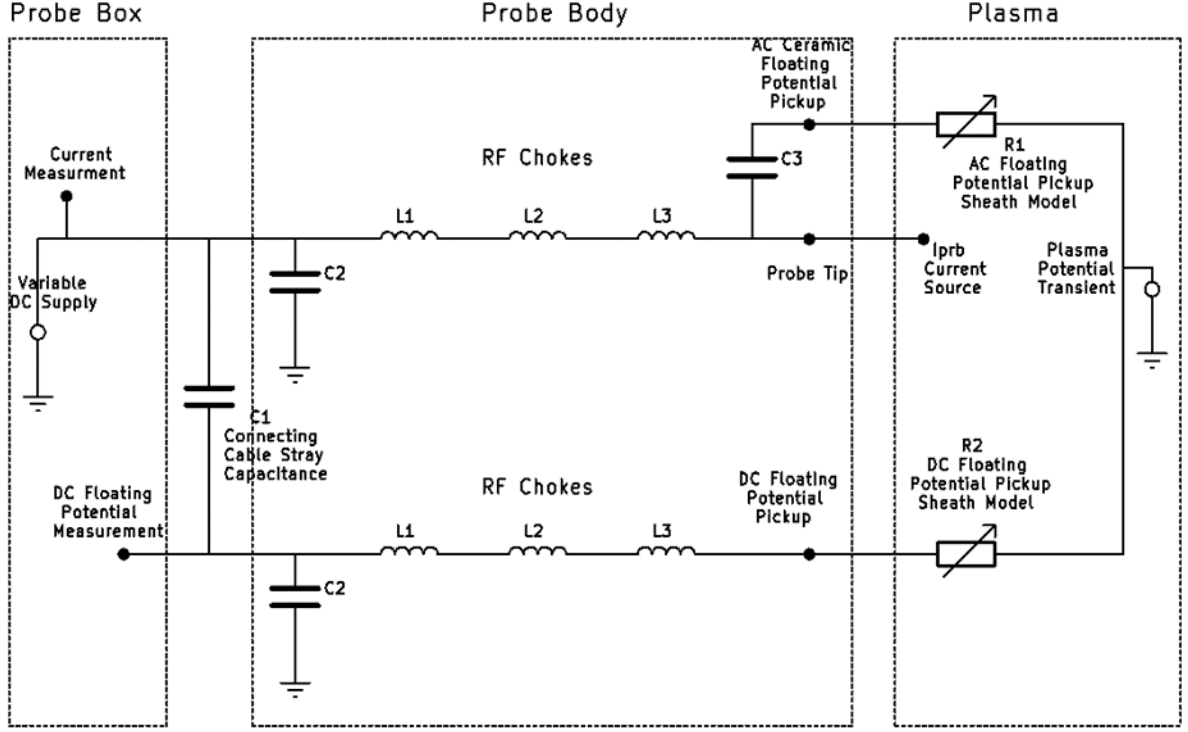
Figure 5.3. Probe circuit model focusing on DC and pulse induced transient voltage current.

because at low frequency or DC, the capacitors look like opens and the inductive components dominate the total circuit characteristics. The second change is in how the plasma is modeled. The capacitance of the plasma sheath also now looks like an open. The resistance portion is still important and is modeled by R1 and R2. The current at the probe tip can be modeled using a piecewise function current source and is denoted as i_{prb}. Equations for each are given by Lieberman[4]

$$i_{prb} = i(V_p)e^{\frac{qV_b}{k_B T_e}} \quad \text{for} \quad V_b \leq 0 \tag{5.2}$$

$$i_{prb} = i(V_p)\sqrt{1 + \frac{qV_b}{k_B T_e}} \quad \text{for} \quad V_b \geq 0 \tag{5.3}$$

This represents basic DC operation. The variable DC supply in the plasma represents the transient due to changes in the plasma. Changes here cause a current in the lower circuit which can be passed through C1 and measured by the system.
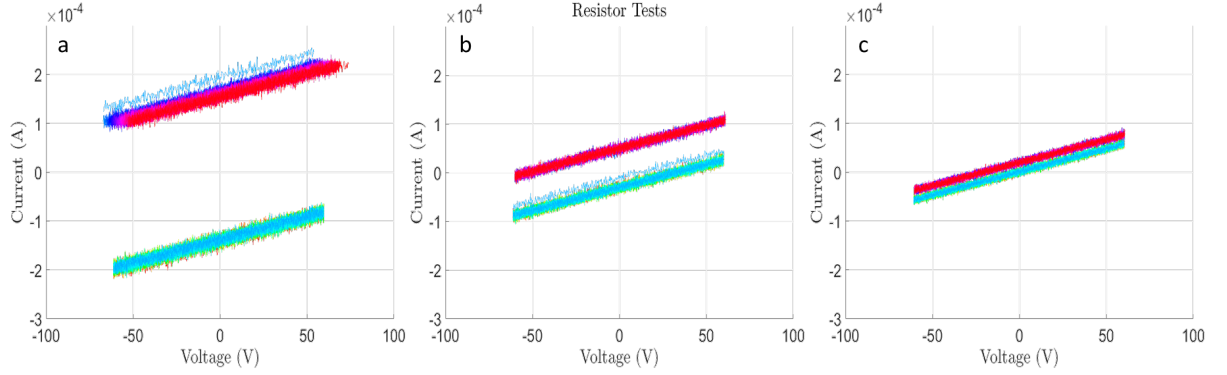
Figure 5.4. Spurious current due to C1. (a) Measured current with a long triax cable. It is seen that there are two sets of currents measured; one during the upslope and one during the downslope of the imposed triangle wave. (b) Measured currents with a short triax cable. As seen, the difference between the measured currents is reduced compared with part a. In part (c) the probe and cables are removed and there is very little capacitive coupling between the two circuits. Therefore the current during both the up and down slope of the triangle wave are very similar.

The majority of the capacitance forming C1 was found to be coming from a long triax cable connecting the LP to the measurement box. To further test this out, the probe was removed from the vacuum chamber and a resistor connected the probe tip to ground. A triangle wave was imposed on the floating probe pickup to simulate a change in V_f. The triangle wave was used as it gives a constant dV/dt during the up and down slopes. Scans were then performed with a long triax (Fig. 5.4 a.) and a short triax (Fig. 5.4 b.). As a control to test the measurement box (Fig. 5.4 c.), the probe was removed. By replacing the long cable with a shorter triax, the induced current was decreased. Removing the probe and connecting cables entirely removed almost all the stray capacitance and reduced the spurious current greatly. Using the equation 5.4 as the current through C1, with dV/dt for a 10 V_{pp} 10 kHz triangle wave found to be $\pm 200000 V/s$, we find $C_{long} = 744\ pF$, $C_{small} = 208\ pF$ and $C_{box} = 50\ pF$.

$$I_{C1} = C1 \frac{dV_{pulse}}{dt} \tag{5.4}$$

40

To keep this capacitance low, the triax cable was replaced with two braided wires. Both the probe circuit wire and the floating electrode circuit wire were twisted with separate ground wires. This setup greatly reduced the capacitive coupling between the two circuits and decreased the induced current in the measurement circuit. This allowed the system to measure accurate IV curves closer to the power turn-on time of the pulse cycle.

Using the theory given and taking the steps mentioned, reasonably accurate plasma parameters can be found using an LP in pulsed plasma. Once these parameters are collected, a better understanding of pulsed plasma conditions can be found. Then the results can be compared with models to improve or lend validity to computer simulations. Finally, verified theory and simulations can be used when designing plasma reactors for semiconductor processing.

REFERENCES

[1] R. Püttner, X.-J. Liu, H. Fukuzawa, T. Tanaka, M. Hoshino, H. Tanaka, J. Harries, Y. Tamenori, V. Carravetta, and K. Ueda, "Potential energy curves of the quasi-stable states of co 2+ determined using auger spectroscopy," *Chemical Physics Letters*, vol. 445, no. 1, pp. 6–11, 2007.

[2] N. G. Einspruch and D. M. Brown, *Plasma processing for VLSI.* Academic Press, 2014, vol. 8.

[3] F. F. Chen, "Industrial applications of low-temperature plasma physics," *Physics of Plasmas*, vol. 2, no. 6, pp. 2164–2175, 1995.

[4] M. A. Lieberman and A. J. Lichtenberg, *Principles of plasma discharges and materials processing.* John Wiley & Sons, 2005.

[5] D. J. Economou, "Pulsed plasma etching for semiconductor manufacturing," *Journal of Physics D: Applied Physics*, vol. 47, no. 30, p. 303001, 2014.

[6] V. Ishchuk, B. E. Volland, M. Hauguth, M. Cooke, and I. W. Rangelow, "Charging effect simulation model used in simulations of plasma etching of silicon," *Journal of Applied Physics*, vol. 112, no. 8, p. 084308, 2012.

[7] S. Samukawa, M. Hori, S. Rauf, K. Tachibana, P. Bruggeman, G. Kroesen, J. C. Whitehead, A. B. Murphy, A. F. Gutsol, S. Starikovskaia *et al.*, "The 2012 plasma roadmap," *Journal of Physics D: Applied Physics*, vol. 45, no. 25, p. 253001, 2012.

[8] C. J. Choi, O. S. Kwon, and Y. S. Seol, "Negative ion formation in sio2 etching using a pulsed inductively coupled plasma," *Japanese journal of applied physics*, vol. 37, no. 12S, p. 6894, 1998.

[9] S. Banna, A. Agarwal, G. Cunge, M. Darnon, E. Pargon, and O. Joubert, "Pulsed high-density plasmas for advanced dry etching processes," *Journal of Vacuum Science & Technology A: Vacuum, Surfaces, and Films*, vol. 30, no. 4, p. 040801, 2012.

[10] J. Poulose, "Temporally, spatially and spectrally resolved studies of pulsed capacitively coupled plasmas," Ph.D. dissertation, The University of Texas at Dallas, 2016.

[11] M. Goeckner, J. Marquis, B. Markham, A. Jindal, E. Joseph, and B.-S. Zhou, "Modified gaseous electronics conference reference cell for the study of plasma-surface-gas interactions," *Review of scientific instruments*, vol. 75, no. 4, pp. 884–890, 2004.

[12] J. L. Kleber and L. J. Overzet, "Sheath resistance measurements in the gec reference reactor," *Plasma Sources Science and Technology*, vol. 8, no. 4, p. 534, 1999.

[13] H. M. Mott-Smith and I. Langmuir, "The theory of collectors in gaseous discharges," *Physical review*, vol. 28, no. 4, p. 727, 1926.

[14] J. Allen, R. Boyd, and P. Reynolds, "The collection of positive ions by a probe immersed in a plasma," *Proceedings of the Physical Society. Section B*, vol. 70, no. 3, p. 297, 1957.

[15] I. B. Bernstein and I. N. Rabinowitz, "Theory of electrostatic probes in a low-density plasma," *The Physics of Fluids*, vol. 2, no. 2, pp. 112–121, 1959.

[16] J. G. Laframboise, "Theory of spherical and cylindrical langmuir probes in a collisionless, maxwellian plasma at rest," Toronto University Downsview (Ontario) INST For Aerospace Studies, Tech. Rep., 1966.

[17] A. Guthrie and R. K. Wakerling, *The characteristics of electrical discharge in magnetic fields*. McGraw-Hill, 1949, vol. 5.

[18] F. F. Chen, "Langmuir probe diagnostics," in *IEEE-ICOPS Meeting, Jeju, Korea*, vol. 2, no. 6, 2003.

[19] ——, "Numerical computations for ion probe characteristics in a collisionless plasma," *Journal of Nuclear Energy. Part C, Plasma Physics, Accelerators, Thermonuclear Research*, vol. 7, no. 1, p. 47, 1965.

[20] A. Rousseau, E. Teboul, and S. Béchu, "Comparison between langmuir probe and microwave autointerferometry measurements at intermediate pressure in an argon surface wave discharge," *Journal of applied physics*, vol. 98, no. 8, p. 083306, 2005.

[21] Z. Zakrzewski and T. Kopiczynski, "Effect of collisions on positive ion collection by a cylindrical langmuir probe," *Plasma Physics*, vol. 16, no. 12, p. 1195, 1974.

[22] M. Tichỳ, M. Šícha, P. David, and T. David, "A collisional model of the positive ion collection by a cylindrical langmuir probe," *Contributions to Plasma Physics*, vol. 34, no. 1, pp. 59–68, 1994.

[23] A. P. Paranjpe, J. P. McVittie, and S. A. Self, "A tuned langmuir probe for measurements in rf glow discharges," *Journal of Applied Physics*, vol. 67, no. 11, pp. 6718–6727, 1990.

[24] M. Hopkins and W. Graham, "Langmuir probe technique for plasma parameter measurement in a medium density discharge," *Review of scientific instruments*, vol. 57, no. 9, pp. 2210–2217, 1986.

[25] G. Narasimhan and C. Steinbrüchel, "Analysis of langmuir probe data: Analytical parametrization, and the importance of the end effect," *Journal of Vacuum Science & Technology A: Vacuum, Surfaces, and Films*, vol. 19, no. 1, pp. 376–378, 2001.

[26] S. Klagge and M. Tichỳ, "A contribution to the assessment of the influence of collisions on the measurements with langmuir probes in the thick sheath working regime," *Czechoslovak journal of physics*, vol. 35, no. 9, pp. 988–1006, 1985.

[27] M. Šícha, P. Špatenka, and M. Tichỳ, "Langmuir probe determination of charged particles density in an rf discharge," *Contributions to Plasma Physics*, vol. 31, no. 1, pp. 43–47, 1991.

[28] J. F. Waymouth, "Perturbation of electron energy distribution by a probe," *Journal of Applied Physics*, vol. 37, no. 12, pp. 4492–4497, 1966.

[29] A. Rousseau, E. Teboul, N. Lang, M. Hannemann, and J. Röpcke, "Langmuir probe diagnostic studies of pulsed hydrogen plasmas in planar microwave reactors," *Journal of applied physics*, vol. 92, no. 7, pp. 3463–3471, 2002.

BIOGRAPHICAL SKETCH

After high school Alex Press joined the navy as an aviation electrician. After four years in the navy, Alex attended Tidewater Community College before transferring to the University of Illinois where in 2014 he earned a BS in physics. During his time at the University of Illinois Alex worked as an undergraduate researcher at the Center for Plasma-Material Interactions. His efforts there culminated in him being named the University of Illinois student worker of the year for 2014. At the start of 2015 Alex joined the Center for Advanced Materials Processing at The University of Texas at Dallas where he works as a graduate research assistant.

Alex F. Press

Contact Information:

Department of Electrical Engineering

The University of Texas at Dallas

800 W. Campbell Rd.

Richardson, TX 75080-3021, U.S.A.

Email: `axp151230@utdallas.edu`

Educational History:

B.S., Physics, University of Illinois, 2014
Ph.D., Electrical Engineering, The University of Texas at Dallas –in progress

Laboratory Experience:

Graduate Research Assistant, The University of Texas at Dallas, Center for Advanced Materials Processing, 2015–present
Summer Intern at Lam Research, 2016
Undergraduate Research, University of Illinois, Center for Plasma-Material Interactions, 2012-2014

Professional Recognitions and Honors:

Student Employee of the Year, University of Illinois, 2014
Yellow Ribbon Scholarship, 2012
Give 'em Hell Hero, Aviation Intermediate Maintenance Department, USS Harry S. Truman, 2008

Professional Memberships:

American Vacuum Society (AVS), 2015–present

Publications:

P. Fiflis, A Press, W. Xu, D. Andruczyk, D. Curreli, D. N. Ruzic, "Wetting properties of liquid lithium on select fusion relevent surfaces", **2014** *Fusion Engineering and Design, ISSN 0920-3796*